SUPPLEMENTARY FIGURES

Supplementary Figure 1

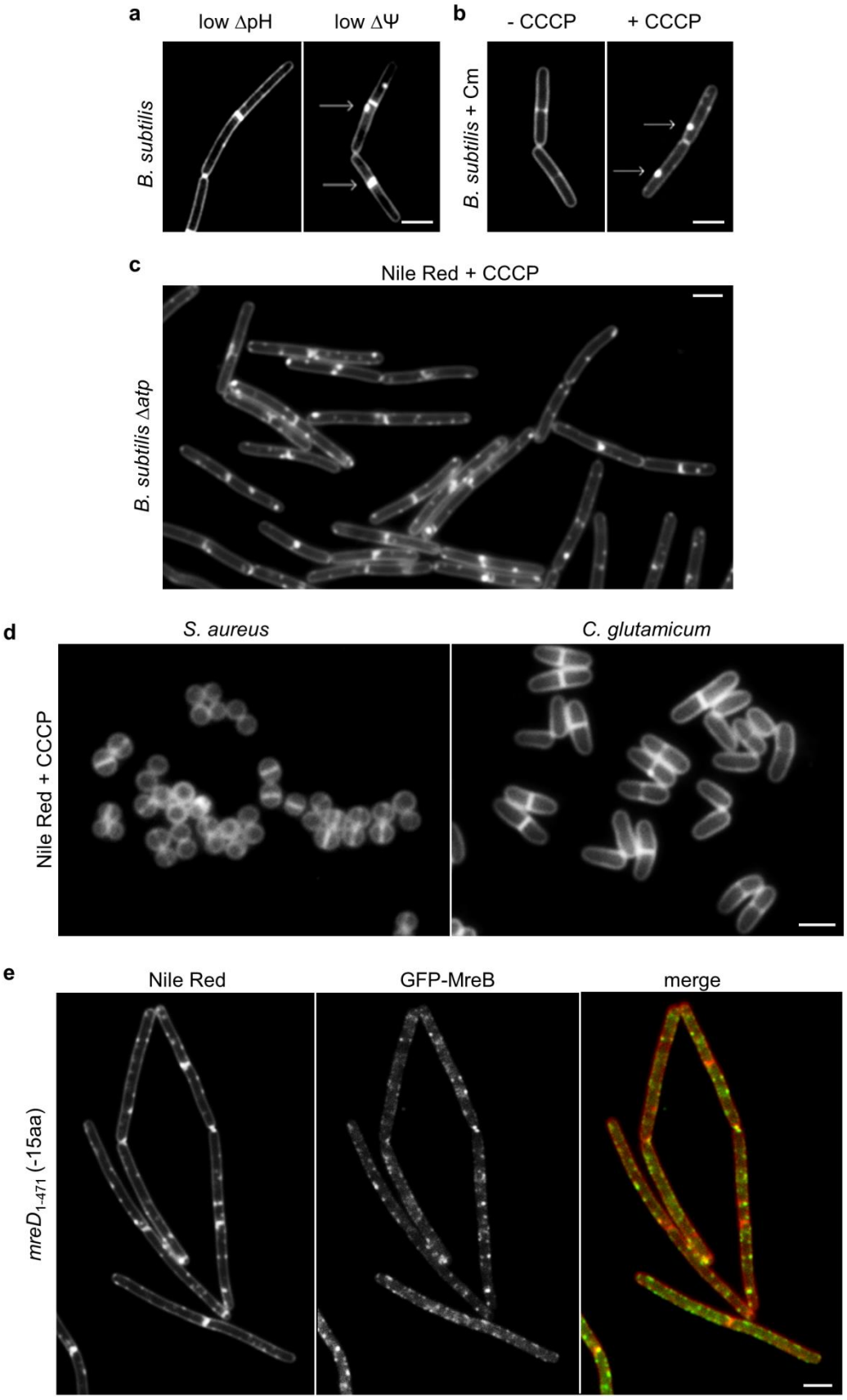

CCCP induced changes in Nile Red stain are caused by delocalization of MreB

(a) CCCP is a specific proton-ionophore that dissipates the proton motive force (pmf), composed of the membrane potential (ΔΨ) and the transmembrane pH gradient (ΔpH). To determine which of these factors is responsible for the irregular Nile Red stain, the membrane potential was dissipated with the K^+ ionophore valinomycin ('low ΔΨ'), and the transmembrane pH gradient by the H^+/K^+ antiporter nigericin ('low ΔpH') [1]. Only dissipation of the ΔΨ triggers the emergence of Nile Red foci (left panels). Some of the Nile Red foci are highlighted with arrows. Strain used: *B. subtilis* 168 wild type. (b) Inhibition of protein synthesis by 5 min pre-incubation with 100 µg/ml chloramphenicol does not prevent CCCP-induced Nile Red foci, indicating that *de novo* protein synthesis is not required. Some of the Nile Red foci are highlighted with arrows. Strain used: *B. subtilis* 168 wild type. (c) Incubation of F_1F_o ATP-synthase deficient cells with CCCP still results in a rapid emergence of Nile Red foci. This is a larger field of cells shown in Figure 1b. Strain used: *B. subtilis* HS13 (Δ*atp*). (d) CCCP does not affect Nile Red fluorescent membrane stain in *Staphylococcus aureus* and *Corynebacterium glutamicum*. This is a larger field of cells shown in Figure 1d. Strains used: *C. glutamicum* RES167, and *S. aureus* RN4220. (e) Colocalization of GFP-MreB with Nile Red foci (middle panel) in *B. subtilis* strain encoding a 15 amino acid C-terminal truncation of MreD (-15aa) that results in a mild delocalization of MreB. This is a larger field of cells shown in Figure 1e. Strain used: *B. subtilis* HS38 *(gfp-mreB mreD1-471*/-15aa). Scale bar, 2 µm.

Supplementary Figure 2

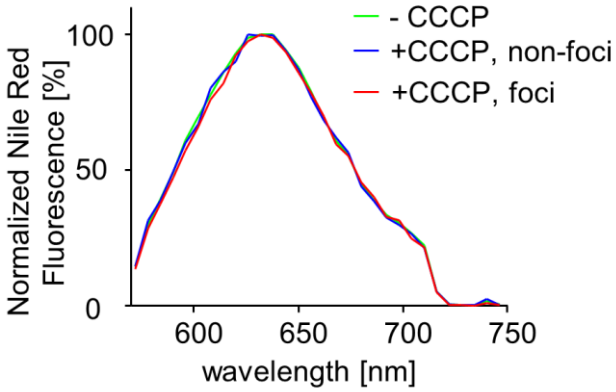

CCCP-induced Nile Red-foci have a regular lipid bilayer structure

The emission spectrum of Nile Red is highly sensitive to its environment and exhibits specific spectral shifts that are commonly used to detect and identify changes in lipid aggregation, and which is used to distinguish the protein and membrane embedded states [2, 3, 4]. To test whether the CCCP-induced Nile Red foci are characterized by binding to protein aggregates, or non-bilayer lipid aggregates, the emission spectrum of Nile red was recorded using spectral imaging fluorescence microscopy. This microscopic technique allows recording of fluorescent wavelength spectra with spatial resolution. The average and normalized spectra of 10 individual CCCP-induced foci are compared against spectra obtained from non-foci areas of CCCP treated cells, and from untreated cells (see Materials and Methods). In all cases, the emission spectra are essentially indistinguishable, indicating that the fluorophore still emits from a regular lipid bilayer environment in the Nile Red foci, and the increased fluorescence is not caused by staining of possible aggregated proteins or lipids. Strain used: *B. subtilis* 168 (wild type).

Supplementary Figure 3

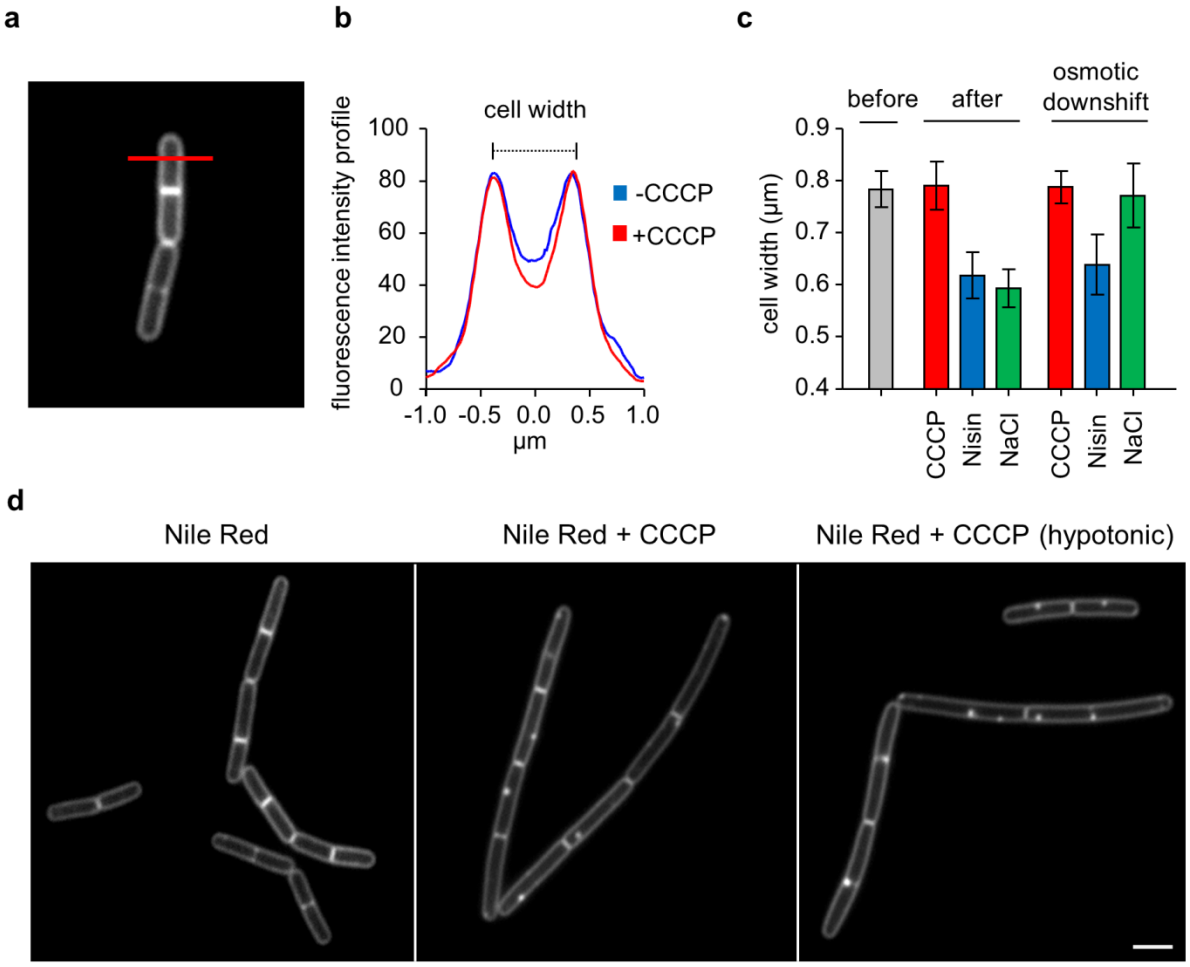

Nile Red foci are not caused by plasmolysis

Rapid loss of cell turgor as a result of CCCP treatment could result in invagination of the cell membrane. To test this possibility, we analysed the cell width that changes as a result of turgor changes. The cell width measurement was based on fluorescent intensity profiles along a line perpendicular to the cell axis (a), with cell width determined as the distance between maxima in membrane fluorescence (b). The average cell width and standard deviation of untreated cells, cells treated with CCCP, Nisin, and 0.5 M NaCl, and treated cells transferred to hypotonic medium (H2O) in order to recover turgor, was measured (n=50 cells) (c). Both Nisin (large pore forming antimicrobial peptide), and osmotic up-shock with 0.5 NaCl were used as positive control to evaluate the ability of our assay to reliably measure changes in cell turgor. No significant effect of CCCP treatment on cell turgor was detected. Finally, if

CCCP-dependent Nile Red-foci were caused by plasmolysis (membrane invagination), transfer to hypotonic environment, which recovers turgor, should reverse the membrane stain back to pre-treatment state. The Nile Red foci are not affected from the hypotonic challenge (d), further indicating that their formation is not related to plasmolysis caused by changes in cell turgor. Strain used: *B. subtilis* 168 (wild type). Scale bar, 2 μm.

Supplementary Figure 4

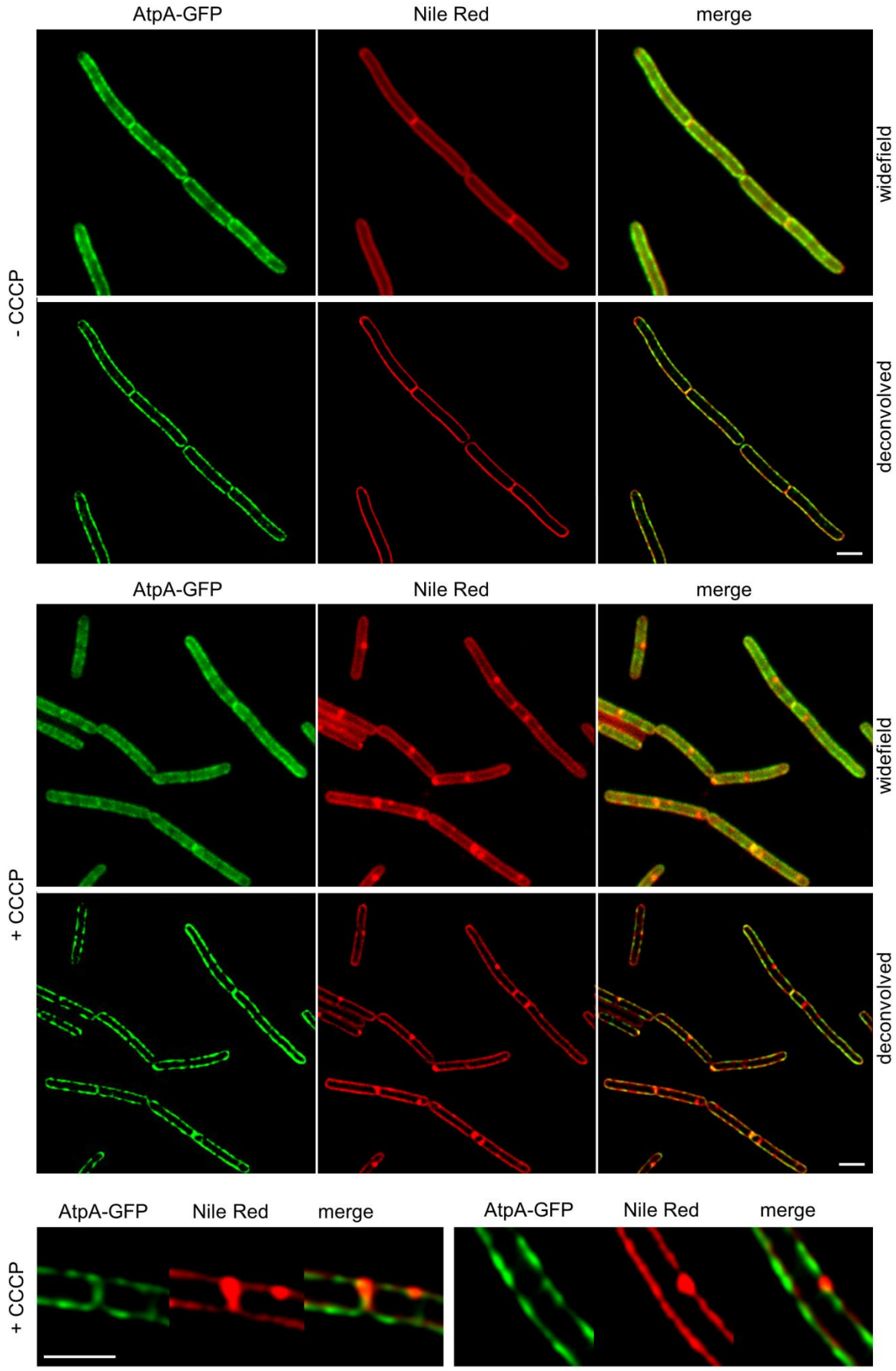

Nile Red foci are not caused by local invagination of the cell membrane

The irregularities in Nile Red membrane staining emerge within minutes, leaving very little time for the synthesis of excess membranes. To confirm that the Nile Red foci are not due to additional membrane layers, e.g. as a consequence of local invagination of the membrane, the localization of an integral membrane protein F_1F_o ATP synthase was determined using a GFP fusion protein (AtpA-GFP). Indeed, this protein does not show any enrichment in membrane areas where Nile Red cluster emerge upon CCCP treatment (middle panels, see lower panels for higher magnification). This rules out the presence of local membrane invaginations upon CCCP treatment. The images were captured as 200 nm optical sections. Both wide field images of the centre plane and the corresponding plane from deconvolved images are depicted in the absence and presence of CCCP. The reason that in some cases the Nile red stain appears to protrude into the cytoplasm is a consequence of high membrane fluorescence originating from slightly above and below the exact focal plane. Strain used: *B. subtilis* BS23 (*atpA-gfp*). Scale bar, 2 μm.

Supplementary Figure 5

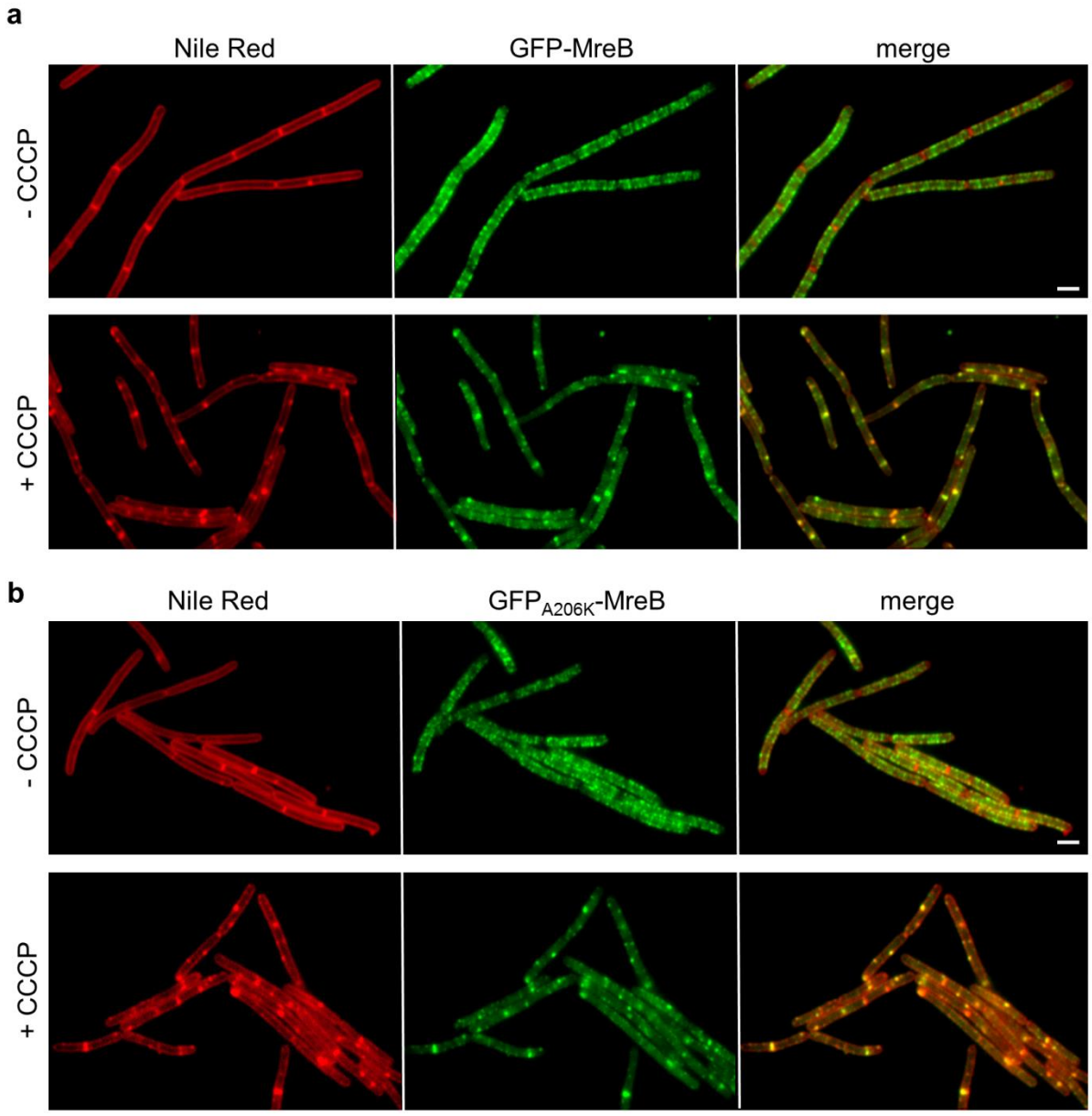

Disruption of the MreB cytoskeleton is accompanied by aberrant membrane stains

(a) Nile Red membrane stained *B. subtilis* cells (left panel) expressing GFP-MreB (middle panel), and merged images are depicted in the absence or presence of the proton ionophore CCCP. This is a larger field of cell shown in Fig. 1a. Strain used: *B. subtilis* YK405 (*gfp-mreB*). (b) Dimerization of GFP was recently shown to cause artificial clustering of certain GFP-fusion proteins (Landgraf *et al,* 2012). To verify that the localization and clustering of GFP-MreB is not influenced by this property, the experiments were repeated with a

monomeric GFP variant (GFP_{A206K}). This gave the same results (panel b). Nile Red membrane stains of *B. subtilis* cells (left panel) expressing GFP_{A206K}-MreB (middle panel), and merged images, are depicted in the absence or presence of the proton ionophore CCCP. The native localization of *B. subtilis* MreB, its delocalization upon CCCP-treatment, and the colocalization with Nile Red foci, is not influenced by the A206K mutation in GFP. Strain used: *B. subtilis* HS37 (*mgfp-mreB*). Scale bar, 2 μm.

Supplementary Figure 6

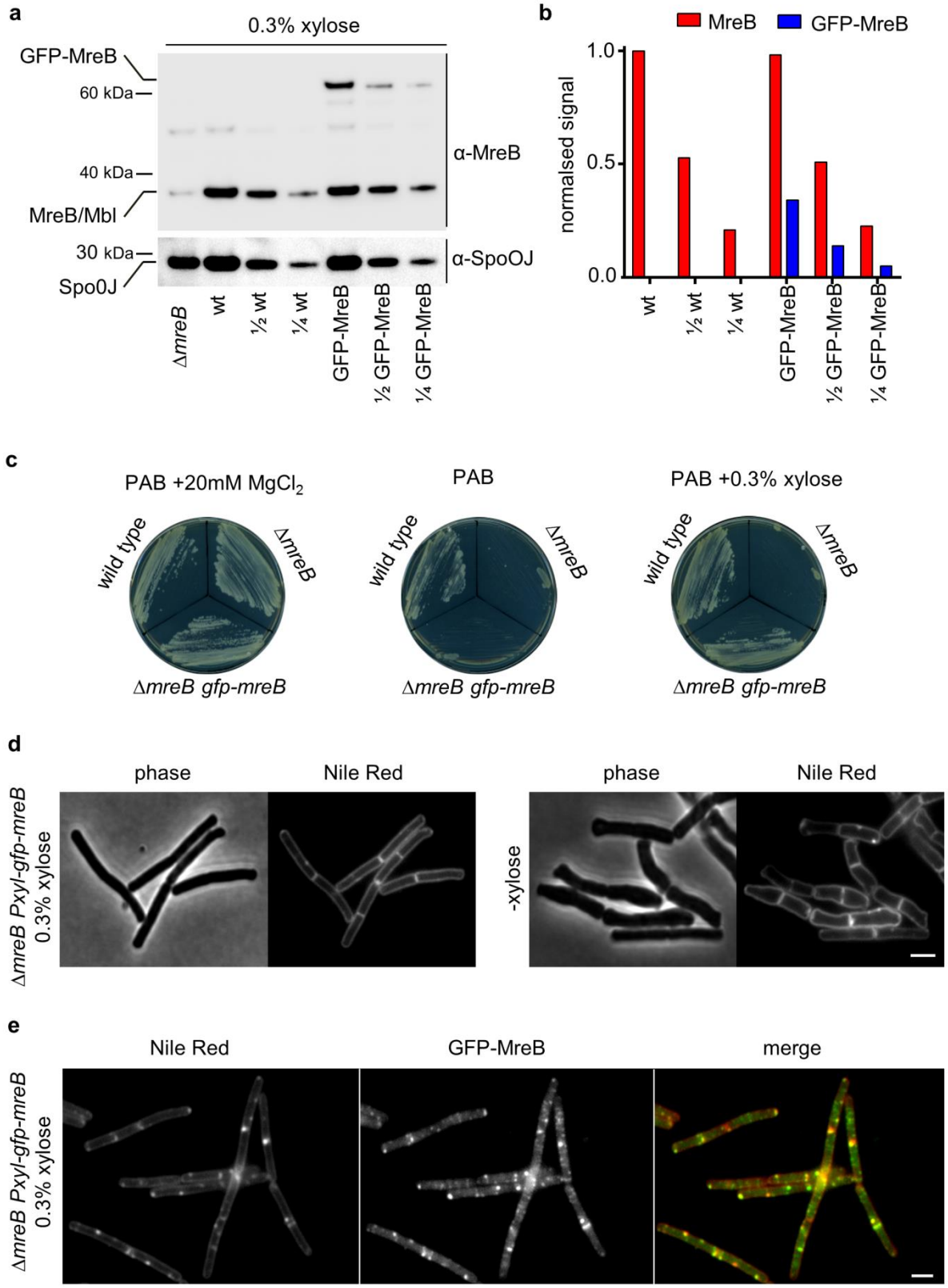

GFP-MreB is active and not overproduced

(a) The expression levels of *gfp-mreB* transcribed from the inducible Pxyl-promoter were compared with native levels of MreB using western blotting. Wild type cells inducing *gfp-mreB* (0.3% xylose, the maximal levels used in this manuscript) were analysed to allow a direct comparison. MreB was detected using polyclonal MreB antibodies. Detection of Spo0J was used as a loading control. To verify that the signals are not saturated, a serial dilution of the samples was performed. Please note that due to high sequence similarity, weak cross-reactivity with Mbl is present. Strains used: *B. subtilis* YK405 (*gfp-mreB*), and 3728 (Δ*mreB*). (b) Densitometric analysis of relative MreB signal intensities reveals that GFP-MreB levels are approximately 30% of the native MreB levels under these induction conditions. (c) GFP-MreB, induced with 0.3% xylose, is able to support growth under conditions in which MreB is essential (PAB-Agar plates without added $MgCl_2$) indicating that the fusion protein is active. (d) GFP-MreB, induced with 0.3% xylose, is able to rescue morphology phenotype of Δ*mreB* (PAB liquid medium, 3h after removal of 20 mM $MgCl_2$). Strain used: *B. subtilis* HS48 (*gfp-mreB,* Δ*mreB*). (e) In the absence of native MreB, GFP-MreB expressed at low levels in LB medium is delocalized by CCCP, and colocalize with Nile Red-foci. Strain used: *B. subtilis* HS48 (*gfp-mreB,* Δ*mreB*). Scale bar, 2 μm. Thus, the delocalization of GFP-MreB by CCCP, and the colocalization with Nile Red-foci, is not caused by overexpression of a non-functional MreB GFP-fusion. Scale bars, 2 μm.

Supplementary Figure 7

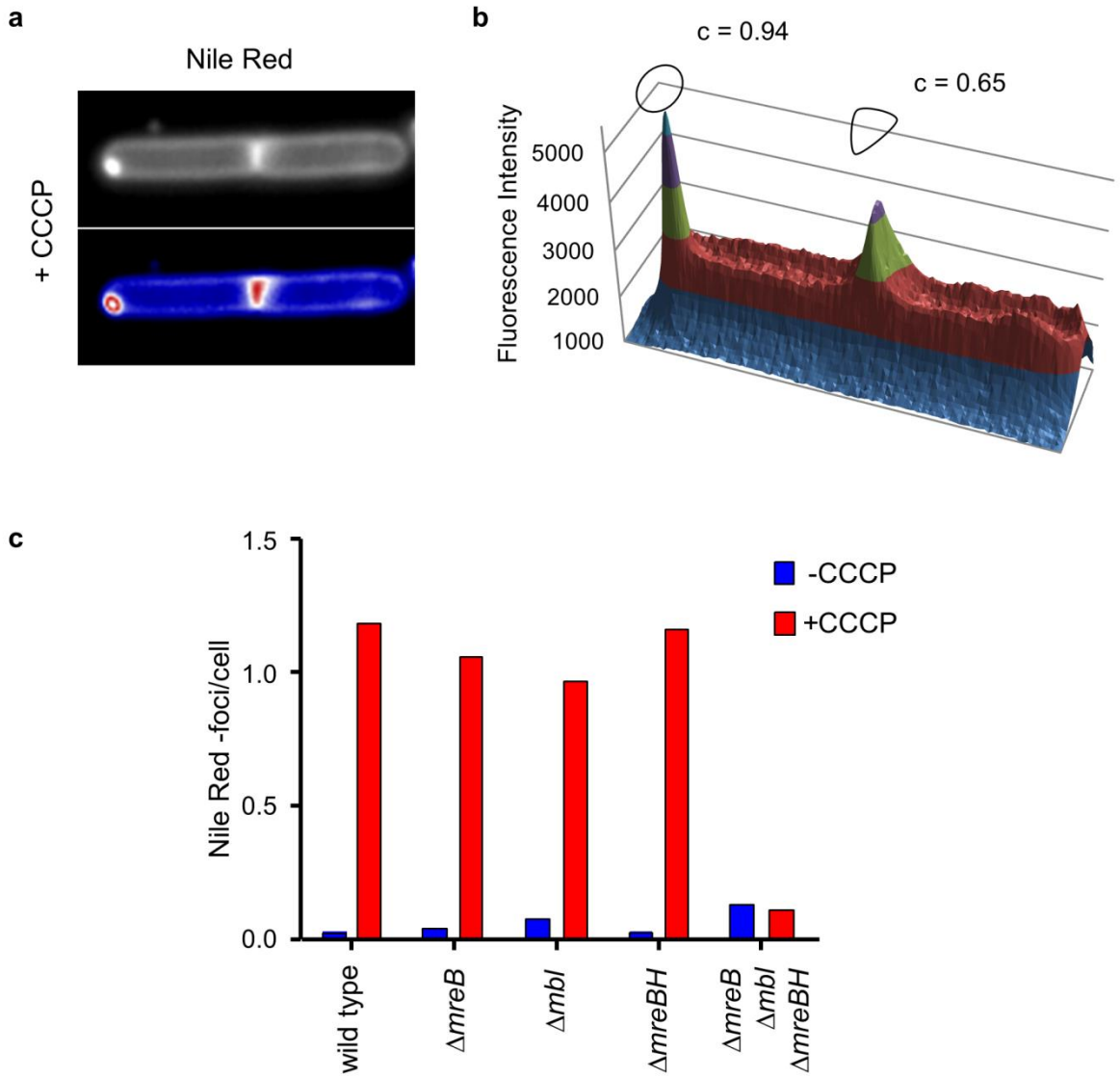

Automated quantification of Nile Red foci –frequency

The frequency of CCCP-induced Nile Red-foci in different strain backgrounds was analysed using an automated detection scheme and ImageJ. (a) An initial screen was performed to identify membrane areas with fluorescent intensities 1.5 times above the average membrane signals, and area between 10 and 100 pixel^2. (b) The detected membrane areas were further divided based on circularity with values above 0.75 regarded as Nile Red –foci, and values below as septa (the presence of two membranes at septum result in higher fluorescence signals). (c) Finally, the frequency of Nile Red-foci was calculated based on manual cell

count of the corresponding image frames. The analysis of rod shaped cells was performed by capturing a single focal plane, and included 355-450 cells. Due to the large round shape of the Δ*mreB* Δ*mbl* Δ*mreBH* –cells, the analysis (190-210 cells) was performed with images captured as 500 nm optical sections. Strains used: *B. subtilis* 168 (wild type), 3728 (Δ*mreB*), 4261 (Δ*mbl*), 4262 (Δ*mreBH*), and 4277 (Δ*mreB*, Δ*mbl*, Δ*mreBH*).

Supplementary Figure 8

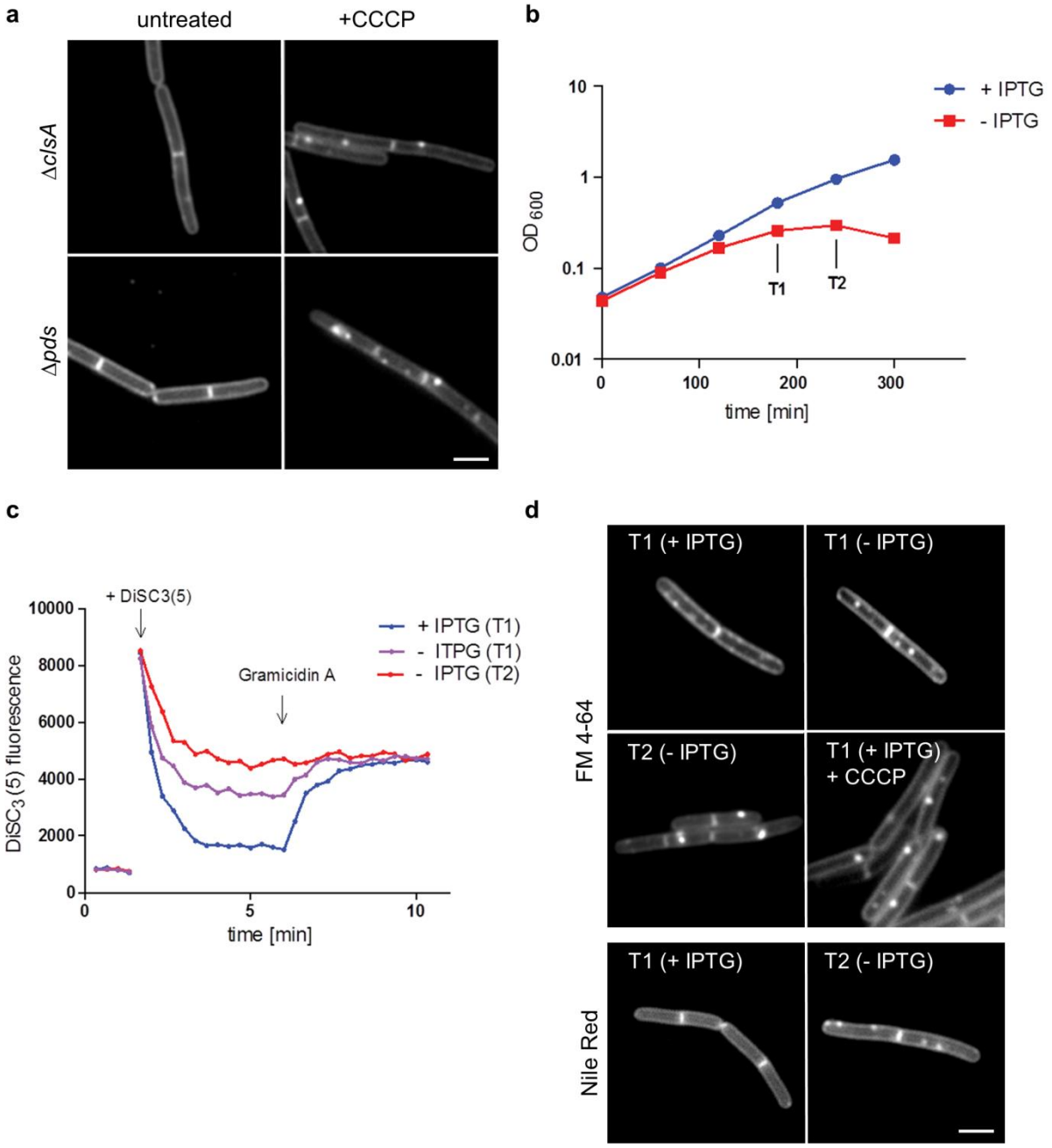

CCCP induced change in the fluorescent membrane stain is independent of lipid head groups

(a) Appearance of Nile Red foci after addition of CCCP in *B. subtilis* strains deficient for cardiolipin (Δ*clsA*) or phosphatidyl ethanolamine (Δ*psd*). Strains used: *B. subtilis* HB5347 (Δ*clsA*) and HB5343 (Δ*psd*). Scale bar, 2 μm. (b) An irregular fluorescent stain in *B. subtilis* cells that weakly resembles a helical pattern has been reported for the membrane dye FM 4-

64 [5, 6]. This was interpreted as phosphatidyl-glycerophosphate (PG) -enriched helical domains, since these structures coalesce when PG is depleted [5]. PG is essential and the most abundant lipid species. Depletion of PG synthase (PgsA) results in an inhibition of growth as shown in panel B (growth curves in the presence (+ IPTG) and absence (- IPTG) of *pgsA*-expression). Time points in which samples were withdrawn for membrane potential measurements (panel C), and microscopy (panel D) are highlighted as T1 and T2. (c) Depletion of PG coincides with dissipation of the membrane potential due to destabilisation of the lipid bilayer barrier function. The cellular membrane potential levels were measured using the fluorescent membrane potential-sensitive dye $DiSC_3(5)$ as described before [1]. Briefly, in the presence of a transmembrane potential the membrane permeable cationic dye $DiSC_3(5)$ accumulates in the cytoplasm. The resulting high local concentration results in quenching of the fluorescence within the cytoplasm. Upon dissipation of the membrane potential with 1 µM Gramicidin A, the dye is released back into the medium. (d) As described before [5], depletion of PgsA results in a change from a weakly helical FM 4-64 membrane stain (T1 + IPTG) to a strongly clustered signal (T1 and T2 – IPTG). However, these irregularities in FM 4-64 stain are also triggered by direct dissipation of the membrane potential with CCCP, even when *pgsA* is expressed (T1 + IPTG and CCCP). Identical clustering upon PgsA depletion (T2 – IPTG) is observed in cells stained with Nile Red as well. Scale bar, 2 µm. Strain used for B-D: *B. subtilis* BFA2809 (*Pspac-pgsA*).. In conclusion, the change of the fluorescent FM 4-64 pattern is due to delocalization of MreB caused by dissipation of membrane potential, and this lipid dye is not an indicator for PG-enriched membrane domains.

Supplementary Figure 9

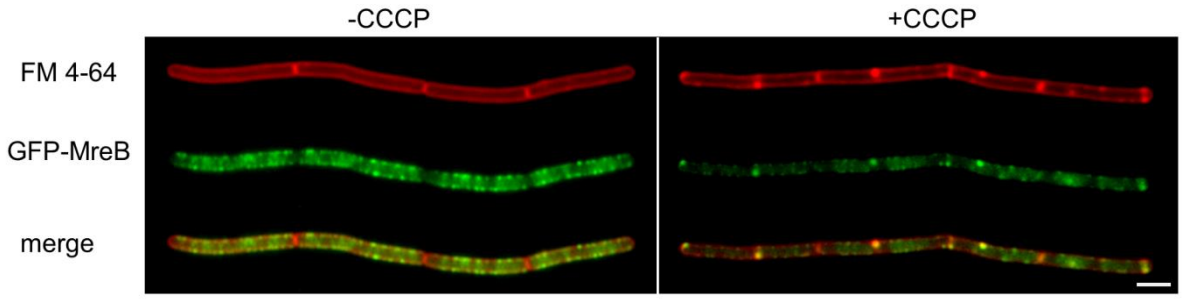

The FM 4-64 foci colocalize with GFP-MreB upon CCCP treatment

FM 4-64 stained *B. subtilis* cells (upper panels) expressing GFP-MreB (middle panels), and merged images (right panels) are depicted in the absence or presence of the proton ionophore CCCP. Strain used: *B. subtilis* YK405 (*gfp-mreB*). Scale bar, 2 μm.

Supplementary Figure 10

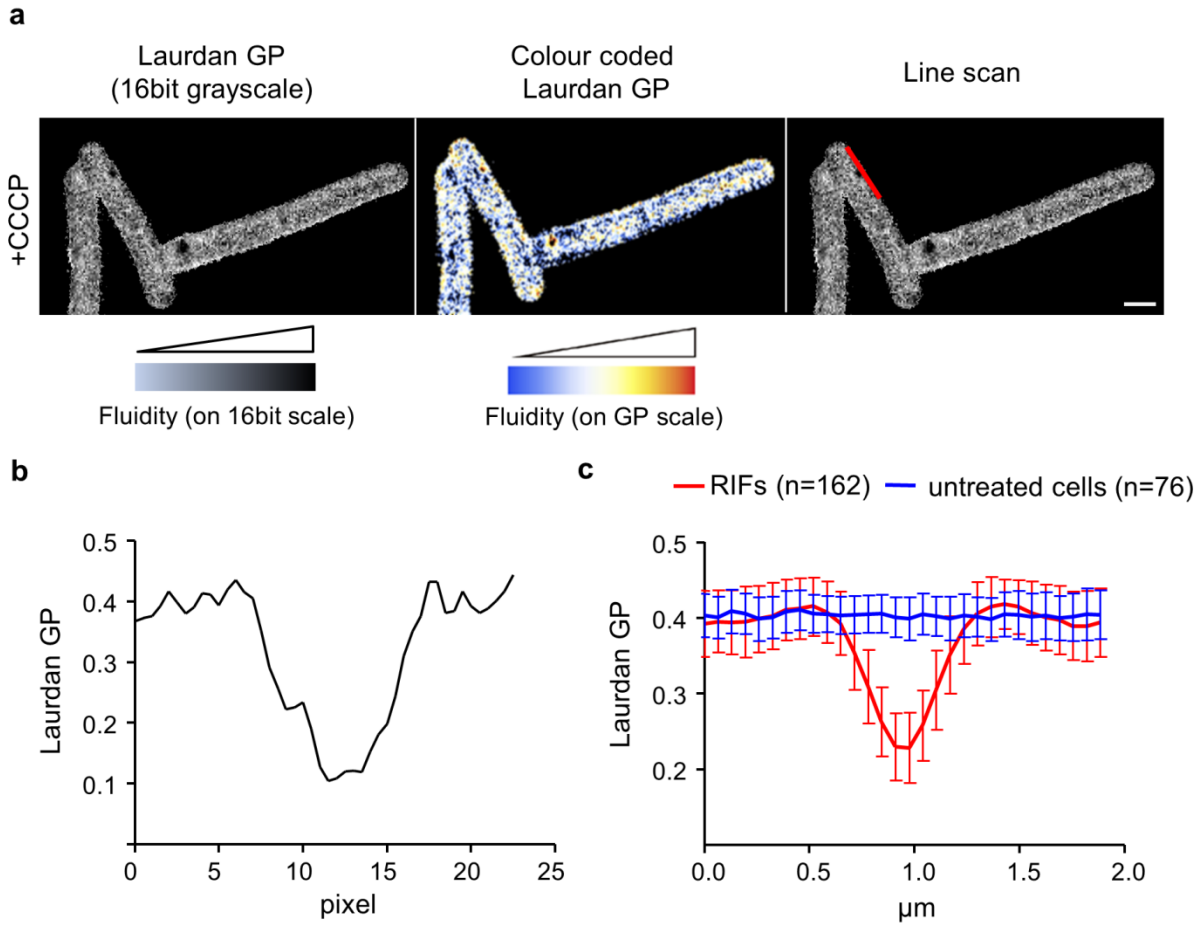

Statistical analysis of changes in local membrane fluidity

To analyse the statistical significance of the detected local changes in membrane fluidity measured as Laurdan generalised polarisation (GP), the RIF-associated change in Laurdan GP was measured using a line scan along the length axis of the cell membrane, centred at RIFs. (a) The analysis was carried out from images in which the Laurdan GP is presented in 16 bit scale (from 0 to 65,536), followed by conversion to GP scale (from -1 to +1). The individual intensity profiles (b) were averaged and are (c) presented as mean and standard deviation for 162 RIFs caused by CCCP treatment, and 76 randomly selected membrane areas of untreated cells. Scale bar, 2 µm. In conclusion, incubation with CCCP generates membrane areas with a significant reduction in 'Laurdan Generalised Polarisation', which indicates an increase in local membrane fluidity.

Supplementary Figure 11

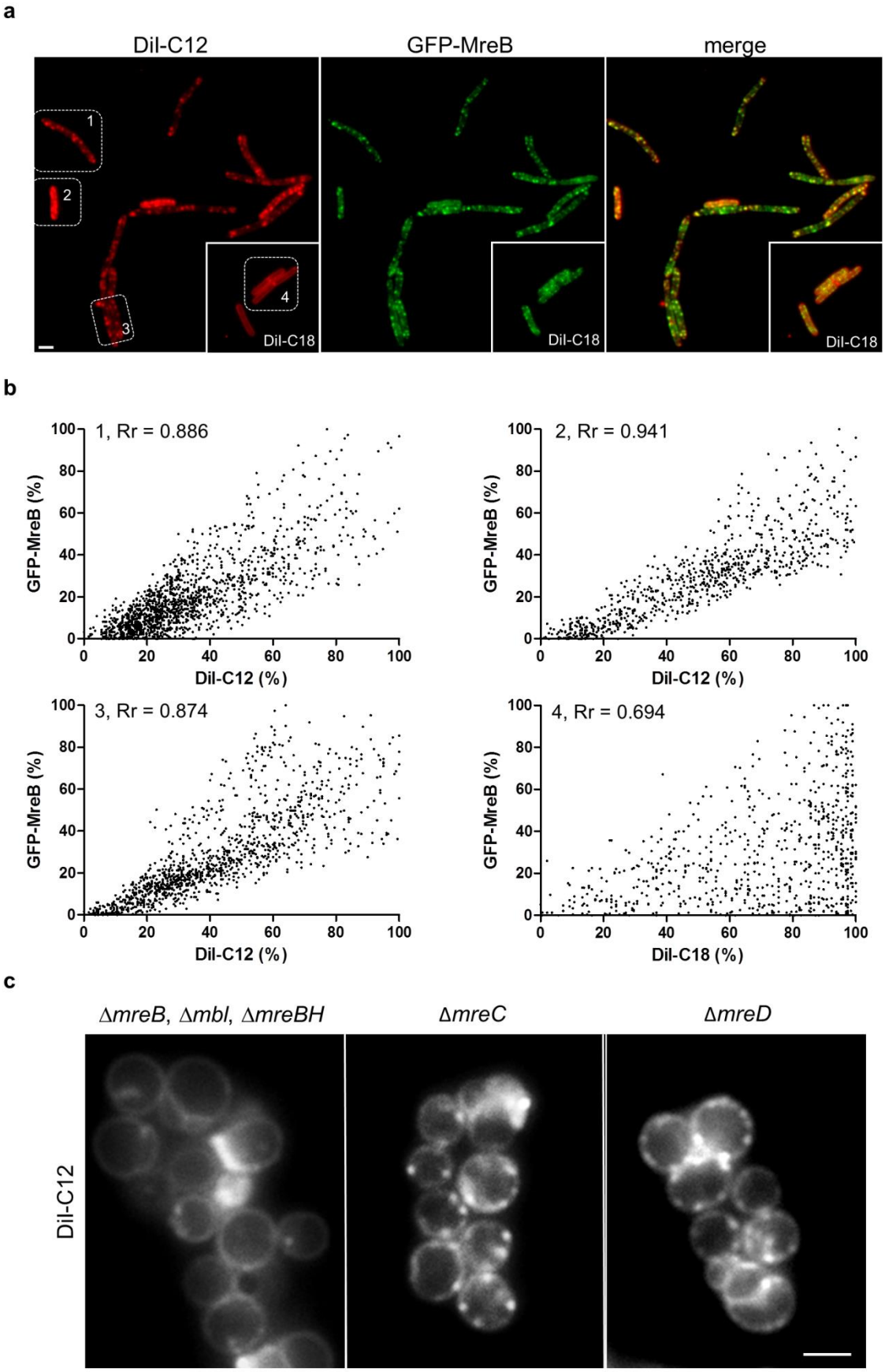

Colocalization of DiI-C12 stained RIFs and GFP-MreB

(a) A field of DiI-C12 membrane stained *B. subtilis* cells (left panel) expressing GFP-MreB (middle panel), and merged images (right panel) is depicted. For comparison, captions of DiI-C18 stained cells are shown in the lower right corners. Strain used: *B. subtilis* YK405 (*gfp-mreB*). This panel shows a larger field of cells shown in Fig. 4b. (b) Fluorescence intensity correlation graphs are shown for 4 random cells in panel B. The graphs display a pixel by pixel intensity correlation between DiI, and GFP-MreB fluorescence. For the analysis, the fluorescence images were background subtracted, and the intensities equalized by conversion into 8 bit images with lowest intensities represented as 0, and highest pixel values as 255. The analyses were carried out using ImageJ "Intensity Correlation Analysis" plugin (Tony Collins, Wright Cell Imaging Facility, Canada) based on Li *et al*, 2004 [7]. The relative intensities are represented as % of the maximal values of the corresponding image fields. Pearson's correlation coefficients, which indicates the significance of correlation on a scale of –1 (full exclusion) to +1 (full correlation), are calculated (Rr). The average Pearson's correlation coefficient for DiI-C12 and GFP-MreB in 19 individual cells was 0.859, indicating a high level of spatial correlation. Importantly, the correlation for DiI-C18 stained cells is significantly lower (Rr = 0.69). It should be mentioned that some fluorescence correlation between DiI-C18 and GFP remains since both DiI-C18 and MreB are present in the cell membrane. (c) DiI-C12 fluorescence images of *B. subtilis* Δ*mreC* and Δ*mreD* cells, and cells that lack the three MreB-homologs (Δ*mreB*, Δ*mbl*, Δ*mreBH*). This is a larger field of cells shown in Figure 5a. Strains used: *B. subtilis* 3481 (Δ*mreC*), 4311 (Δ*mreD*), 4277 (Δ*mreB*, Δ*mbl*, Δ*mreBH*, Δ*rsgI*). Scale bar, 2 μm

Supplementary Figure 12

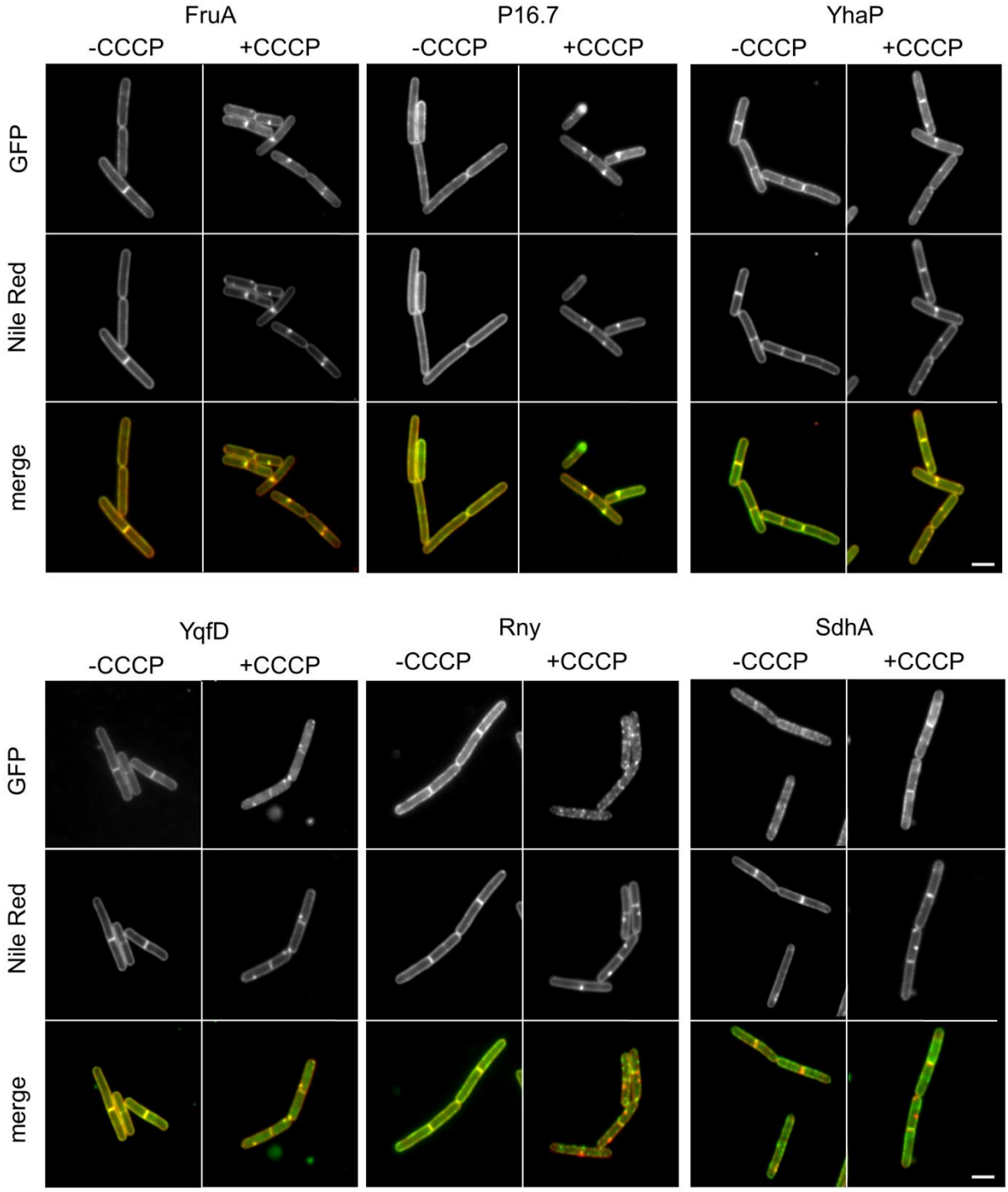

Colocalization of CCCP-induced membrane protein clusters with Nile Red

CCCP induces clustering of several membrane proteins (FruA, P16.7, YhaP, YqfD, and Rny), whereas the localization of other proteins (SdhA, for AtpA see Supplementary Fig. 4) remains unaffected. In case of FruA, P16.7, YhaP and YqfD, the induced clusters colocalize with Nile Red membrane foci. The delocalization of Rny follows a different pattern. In this

case, rather than forming few clusters that overlap with Nile Red-foci, a large number of non-colocalizing clusters are formed. Strains used: *B. subtilis* 3569 (*rny-gfp*), FruA-GFP, 110WA (*p16.7-gfp*), *yhaP-gfp, yqfD-gfp*, and BS112 (*sdhA-gfp*). Scale bar, 2 μm

Supplementary Figure 13

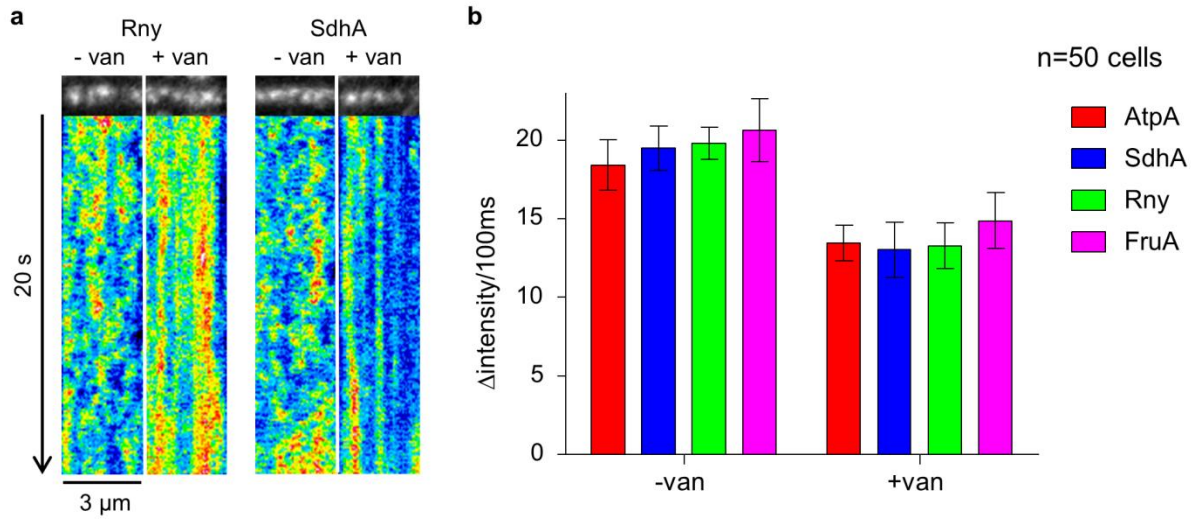

Quantification of vancomycin-inhibited membrane protein mobility

(a) Kymographs visualizing the diffusion of RNaseY (Rny) and Succinate dehydrogenase (SdhA), in the absence and presence of vancomycin, which blocks MreB movement. Time lapse series with 20 s length and 100 ms time resolution were acquired using TIRF microscopy. See movie S5 for corresponding raw image series. Strains used: *B. subtilis* 3569 (*rny-gfp*) and BS112 (*sdhA-gfp*). (b) The statistical significance of the observed reduction in mobility of membrane proteins upon inhibition of MreB-movement was confirmed using fluorescence intensity fluctuation analysis. The movement of a membrane protein with a heterogeneous distribution pattern results in fluctuation of the fluorescence intensity for a given pixel over time, with larger fluctuations reflecting higher mobility. This property also forms the fundamental basis for fluorescence correlation spectroscopy (FCS). We analysed the average time-dependent change in pixel intensity for 50 individual cells in the presence and absence of vancomycin. The pixel intensities were recorded as an average intensity of 3 neighbouring pixels following a 31 pixel long line along the length axis of the cell. The values were normalised through conversion into 8 bit image, which defines the highest intensity values as 256, and the lowest as 0. The intensity fluctuation for each pixel was

calculated as $\Delta I = \left| I(t_n) - I(t_{n+1}) \right|$ for 200 time points (100 ms time resolution). Finally, the individual ΔI -values for 200 time points, 31 pixel values, and 50 cells were averaged and are represented as mean and standard deviation. A clear reduction of intensity fluctuation is observed for cells treated with vancomycin, indicating a significant reduction in mobility. Strains used: *B. subtilis* 3569 (*rny-gfp*), FruA-GFP, 110WA (*p16.7-gfp*), *yhaP-gfp*, *yqfD-gfp*, BS112 (*sdhA-gfp*), and BS23 (*atpA-gfp*).

Supplementary Figure 14

a

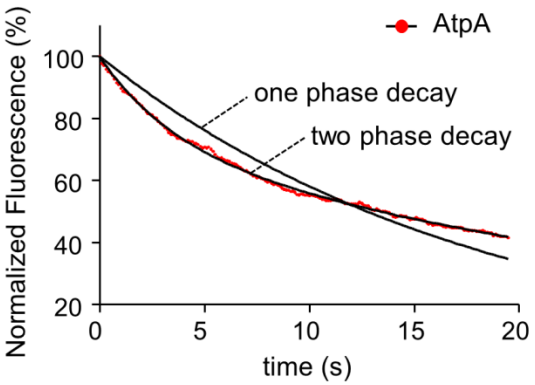

b

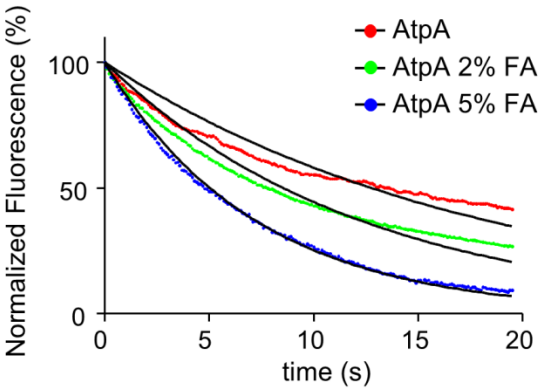

	k (1/s)	SEM	R^2	n (cells)
AtpA	5.44E-02	6.5E-04	0.896	32
AtpA 2% FA	8.12E-02	7.3E-04	0.959	39
AtpA 5% FA	1.38E-01	4.7E-04	0.997	45

c

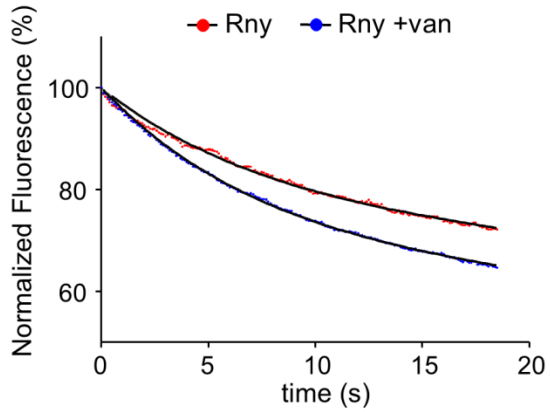

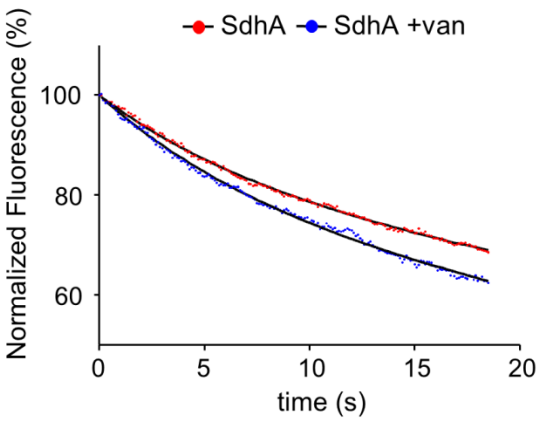

d

	k (1/s)	SEM	R^2	n (cells)
FruA	6.96E-03	4.6E-04	0.988	47
FruA + vancomycin	8.84E-03	3.4E-04	0.997	42
Rny	4.65E-03	3.1E-04	0.993	51
Rny + vancomycin	6.35E-03	1.7E-04	0.999	48
AtpA	5.97E-03	1.9E-04	0.996	52
AtpA + vancomycin	9.43E-03	2.1E-04	0.998	55
SdhA	11.4E-03	2.0E-04	0.998	36
SdhA + vancomycin	14.9E-03	3.3E-04	0.997	37

Quantification of bleaching kinetics

(a) The normalised and background-subtracted GFP fluorescence intensity (AtpA-GFP) follows a biexponential decay from 100 to 0 ($y=y0*e^{(-kfast*x)}+y0*e^{(-kslow*x)}$), with fast rate constant associated with bleaching of GFP within the reach of the evanescent light, and slow rate constant determined by diffusion limited bleaching of the whole cell fluorescence. (b) To verify that biexponential decay is diffusion limited, and to analytically determine the rate constant for direct GFP-bleaching, unfixed samples were compared with samples in which the mobility of the membrane protein was reduced by chemical fixation with formaldehyde. In contrast to unfixed and mildly fixed (2% FA) samples, strong fixation (5% FA) results in bleaching kinetics which follow monoexponential decay ($y=y0*e^{(-k*x)}$) with a single rate constant (0.1378 1/s). (c-d) The analytically determined fast rate constant was used to fit the biexponential decay functions of Fructose permease (FruA), F_1F_o ATP synthase (AtpA) (see Fig. 8b), RNaseY (Rny), and Succinate dehydrogenase (SdhA) (shown here). In all cases, a significant increase in diffusion-limited slow rate constant was observed, which indicates a reduced exchange of proteins between the TIRF-illuminated area, and rest of the cell surface, thus, reduced diffusion rates. Strains used: *B. subtilis* BS23 (*atpA-gfp*), BS112 (*sdhA-gfp*), FruA-GFP, and 3569 (*rny-gfp*).

Supplementary Figure 15

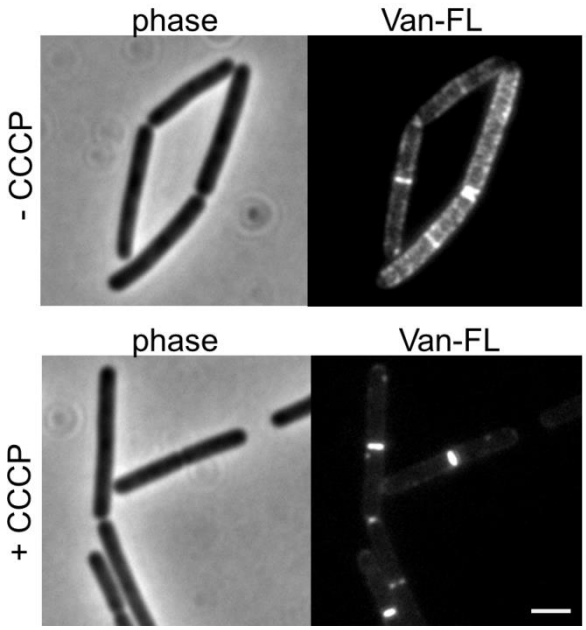

Lipid II levels in the lateral cell wall are reduced by CCCP

Lipid II was stained with fluorescent vancomycin in the absence (left panels) and presence (right panels) of CCCP. In uninhibited cells undergoing cell division and elongation, Lipid II clusters at sites of active cell wall synthesis. The local enrichment of Lipid II in the cylindrical part of the cell (lateral cell wall) requires MreB [8]. Upon CCCP addition, the lateral clusters of Lipid II disappear whereas the septal staining remains unaffected. Strain used: *B. subtilis* 168 (wild type). Scale bar, 2 μm

Supplementary Figure 16

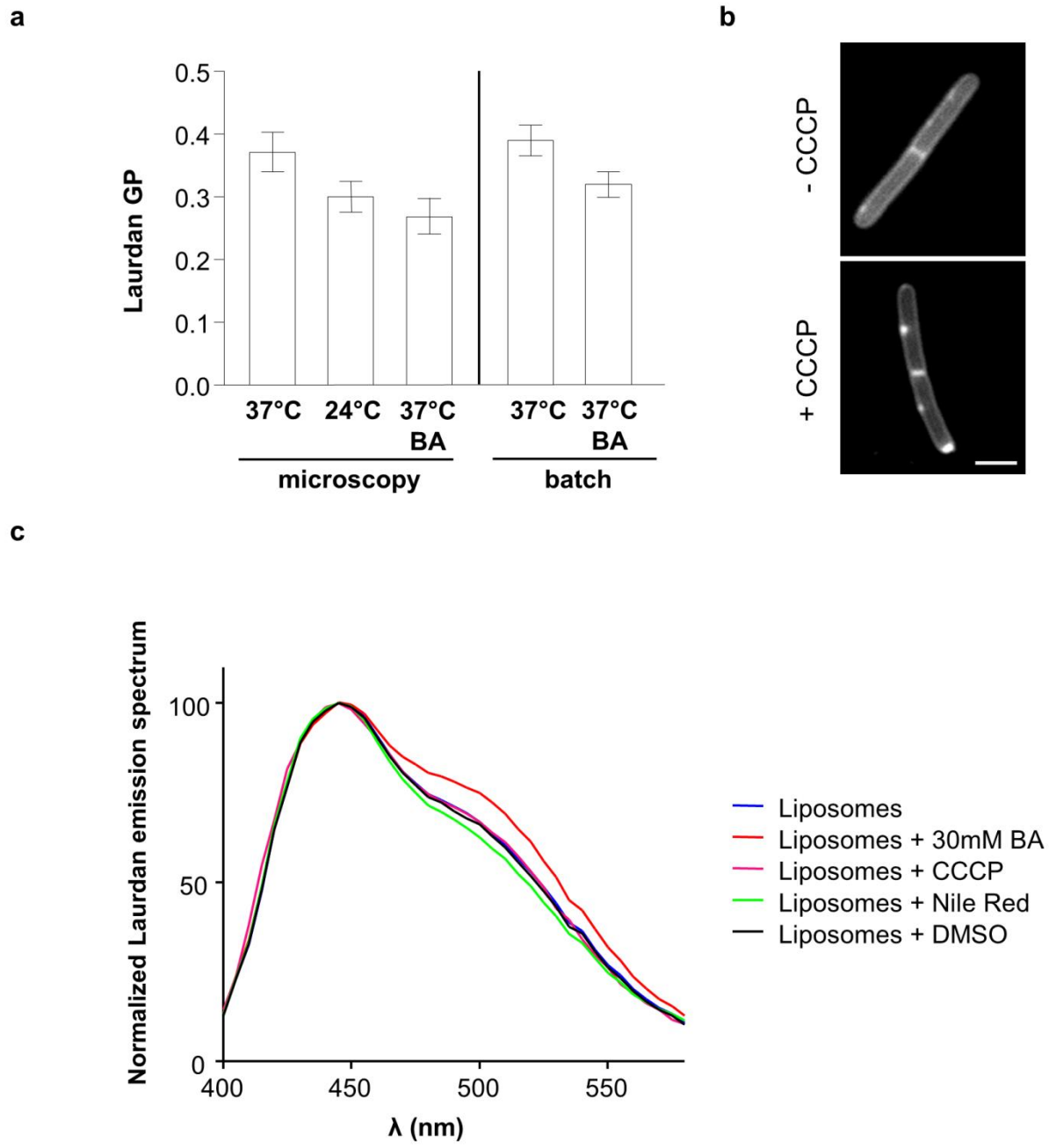

Comparison of Laurdan-based cell membrane fluidity measurements using fluorescence microscopy or fluorometric batch assays, and the influence of compounds on spectral properties of Laurdan

(a) For microscopic analyses, *B. subtilis* cells were grown at 37 ºC or 24 ºC, followed by measurements at 24 ºC. In addition, the membrane fluidity was increased (decrease in Laurdan GP) by addition of 30 mM membrane fluidizer benzyl alcohol (BA). The fluidities

of 70 individual cells were analysed. For batch measurements, the fluidity was determined fluorometrically using cultures that were grown at 37 ºC and incubated for 2 min in the presence or absence of the membrane fluidizer benzyl alcohol (BA). The diagram depicts the average and standard deviation of 3 separate samples. Strain used: *B. subtilis* HB5134 (Δ*des*). (b) The lipid desaturase Des is responsible for rapid unsaturation of phospholipids. As a result of Des activity, elevated levels of fluid lipid species are formed upon cold shock. The formation of CCCP dependent Nile Red foci was independent of Des, indicating that local formation of unsaturated lipid species by Des is not responsible for the formation of RIFs. Strain used: *B. subtilis* HB5134 (Δ*des*). Scale bar, 2 μm (c) As an additional control, we verified that the compounds used in combination with Laurdan do not interfere with the spectral properties of Laurdan. For this, the emission spectrum of Laurdan embedded in liposomes was recorded. The spectra are an average of 3 independent wavelength scans. No significant changes in Laurdan emission spectrum were detected for CCCP, Nile Red, or DMSO (solvent used for CCCP and Nile Red) in the concentrations used in this manuscript. In addition, the positive spectral shift upon addition of 30 mM membrane fluidizer benzyl alcohol (BA) is shown. We conclude that neither CCCP, nor Nile Red interferes with the ability of Laurdan to detect changes in membrane fluidity.

Supplementary Figure 17

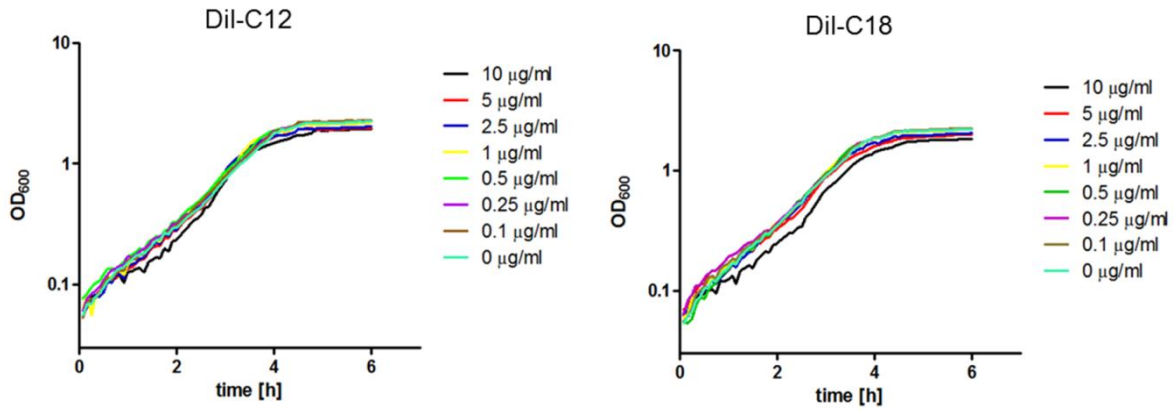

***B. subtilis* growth is not inhibited by DiI-C12 or DiI-C18**

B. subtilis wild type cells were grown in microtiter plates with increasing concentrations of DiI-C12 or DiI-C18. The concentration of the solvent DMSO was maintained constant at 1%. No growth inhibitory effect was detected with 2-4 -fold higher concentrations than used for staining cell membranes (2.5-5 µg/ml).

SUPPLEMENTARY TABLES

Supplementary Table 1: Fatty acid profile, and changes in membrane fluidity of Δ*mre* strains

Fatty acid	wild type	Δ*rsgI*	Δ*mreC*	Δ*mreB**
$C_{14:0}$	**1.2** ±0.11	**1.0** ±0.00	<1	<1
$C_{14:0}$ *iso*	**1.7** ±0.21	**1.7** ±0.03	<1	<1
$C_{15:0}$ *iso*	**20.8** ±1.11	**19.6** ±0.17	**13.5** ±0.04	**16.7** ±0.01
$C_{15:0}$ *anteiso*	**37.6** ±2.42	**35.2** ±0.40	**37.4** ±0.08	**36.3** ±0.03
$C_{16:0}$	**6.5** ±0.25	**6.6** ±0.07	**7.0** ±0.04	**6.0** ±0.01
$C_{16:0}$ *iso*	**4.1** ±0.09	**4.6** ±0.01	**3.0** ±0.00	**2.3** ±0.02
$C_{17:0}$ *iso*	**11.2** ±0.95	**12.3** ±0.31	**14.7** ±1.44	**17.5** ±0.00
$C_{17:0}$ *anteiso*	**10.6** ±0.86	**11.0** ±0.26	**17.9** ±0.31	**16.6** ±0.03
$C_{18:0}$	**1.4** ±0.17	**1.5** ±0.09	**2.2** ±0.07	**1.6** ±0.02
$C_{18:1}$	**3.2** ±0.45	**3.3** ±0.04	<1	<1
sum	98.1 %	96.8 %	95.7 %	97.1 %
C17/C15	**0.37** ±0.05	**0.42** ±0.01	**0.64** ±0.01	**0.65** ±0.01
iso/anteiso	**0.78** ±0.03	**0.83** ±0.01	**0.57** ±0.00	**0.69** ±0.00
Laurdan GP	**0.44** ±0.02	**0.44** ±0.01	**0.43** ±0.02	**0.35** ±0.02

The fraction of fatty acids which contribute to more than 1% of the overall fatty acid content are presented as mean and standard deviation of duplicate measurements. The corresponding *in vivo* Laurdan GP values are presented as mean and standard deviation of three independent measurements. Strains used: *B. subtilis* 168 (wild type), 4264 (Δ*rsgI*), 3481 (Δ*mreC*), 4277/Δ*mreB** (Δ*mreB*, Δ*mbl*, Δ*mreBH*, Δ*rsgI*).

Supplementary Table 2: Strains

Strain	Genotype/Properties	Induction	Source
B. subtilis 168	*trpC2* wild type	-	9
B. subtilis HS13	*ery atpB:pMutin4*	-	1
B. subtilis 3728	*Ωneo3427 ΔmreB*	-	10
B. subtilis 4261	*cat Δmbl*	-	11
B. subtilis 4262	*ery ΔmreBH*	-	11
B. subtilis 4277	*Ωneo3427 ΔmreB Δmbl::cat ΔmreBH::erm Ω(neo::spc) ΔrsgI*	-	11
B. subtilis 4264	*ΔrsgI::spc*	-	11
B. subtilis YK405	*spc amyE::Pxyl-gfp-mreB*	0.1-0.3 % xylose	12
B. subtilis HS37	*spc amyE::Pxyl-mgfp-mreB*	0.1 % xylose	this work
B. subtilis HS48	*spc amyE::Pxyl-gfp-mreB Ωneo3427 ΔmreB*	0.3% xylose	this work
B. subtilis RD159	*neo rodA::Pspac-rodA*	0-100 µM IPTG	R. Daniel, unpublished
B. subtilis BS23	*cat atpA-gfp:Pxyl-'atpA*	0.5% xylose	13
B. subtilis BS112	*cat sdhA-gfp:Pxyl-'sdhA*	0.5% xylose	13
B. subtilis 110WA	*spc amyE::Pxyl-p16.7-gfp*	0.3% xylose	14
B. subtilis FruA-GFP	*spc amyE::Pxyl-fruA-gfp*	1% xylose	15
B. subtilis YhaP-GFP	*spc amyE::Pxyl-yhaP-gfp*	1% xylose	15
B. subtilis YqfD-GFP	*spc amyE::Pxyl-yqfD-gfp*	1% xylose	15
B. subtilis 3569	*spc amyE::Pxyl-rny-gfp*	1% xylose	16
B. subtilis HB5347	*tet ΔclsA*	-	17
B. subtilis HB5343	*ery Δpsd*	-	17
B. subtilis HB5134	*spc Δdes*	-	18
B. subtilis HS31	*ery mreD:pMutin4 (mreD1-172)*	-	this work
B. subtilis HS32	*ery mreD:pMutin4 (mreD1-157)*	-	this work
B. subtilis HS33	*ery spc mreD:pMutin4 (mreD1-172) amyE::Pxyl-gfp-mreB*	0.1% xylose	this work
B. subtilis HS34	*ery spc mreD:pMutin4 (mreD1-157) amyE::Pxyl-gfp-mreB*	0.1% xylose	this work
B. subtilis HS35	*spc neo amyE::Pxyl-gfp-mreB ΔmreBCD*	0.3% xylose	this work
B. subtilis BFA2809	*ery pgsA::pMutin4*	0-100 µM IPTG	19
B. subtilis HS36	*spc neo amyE::Pxyl-gfp-mreB rodA::Pspac-rodA*	0.3% xylose 0-100 µM IPTG	this work
B. subtilis HS38	*tet amyE::Pxyl-rny-gfp*	1% xylose	this work
B. subtilis HS39	*tet amyE::Pxyl-fruA-gfp*	1% xylose	this work
B. subtilis HS40	*tet amyE::Pxyl-p16.7-gfp*	1% xylose	this work
B. subtilis HS41	*tet amyE::Pxyl-yhaP-gfp*	1% xylose	this work
B. subtilis HS42	*tet amyE::Pxyl-yqfD-gfp*	1% xylose	this work
B. subtilis HS43	*tet amyE::Pxyl-rny-gfp Ωneo3427ΔmreB Δmbl::cat ΔmreBH::erm ΔrsgI::spc*	1% xylose	this work
B. subtilis HS44	*tet amyE::Pxyl-fruA-gfp Ωneo3427ΔmreB Δmbl::cat ΔmreBH::erm ΔrsgI::spc*	1% xylose	this work
B. subtilis HS45	*tet amyE::Pxyl-p16.7-gfp Ωneo3427ΔmreB Δmbl::cat ΔmreBH::erm ΔrsgI::spc*	1% xylose	this work
B. subtilis HS46	*tet amyE::Pxyl-yhaP-gfp Ωneo3427ΔmreB Δmbl::cat ΔmreBH::erm ΔrsgI::spc*	1% xylose	this work
B. subtilis HS47	*tet amyE::Pxyl-yqfD-gfp Ωneo3427ΔmreB Δmbl::cat ΔmreBH::erm ΔrsgI::spc*	1% xylose	this work
C. glutamicum RES167		-	20
S. aureaus RN4220		-	21

Supplementary Table 3: Oligonucleotides

Oligonucleotide	Sequence
mreD-for	GCGCGAAGCTTTAACAGATGACCAAGTGCTCGCC
mreD-rev 1-172	GCGCGGGATCCTTACTCATCTCTCAATTCTTTCTTTAG
mreD-rev 1-157	GCGCGGGTACCTTATGGCAGAACAAGAATAAGAGC
GFPA206K-for	CCTGTCCACACAATCTAAACTTTCGAAAGATCCC
GFPA206K-rev	GGGATCTTTCGAAAGTTTAGATTGTGTGGACAGG
pSG1154-for	GCTAATTTTATTGCAATAACAGGTG
pSG1154-rev	GACCGTTAGCGTTTAAGTACATC
tetR-for	TGCAATAAAATTAGCCTGCAGGTCGATATGAACAGC
tetR-rev	TAAACGCTAACGGTCCTCTCTCCCAAAGTTGATCC
pSG1154-for2	GAACTATACAAATAAATGTCCAGAC
pSG1154-rev2	CCGACAGGCTTTGAAGCATG
Pxyl-for	TTCAAAGCCTGTCGGAATTGG
GFP-rev	TTATTTGTATAGTTCATCCATGCC

SUPPLEMENTARY METHODS

Bacterial strains and growth conditions

The used strains, and conditions for gene induction are listed in Table S2. All *B. subtilis* strains were grown in the absence of antibiotics in LB medium at 30 °C, if not stated otherwise. LB supplemented with 20 mM $MgCl_2$ was used to grow the *mreB, mbl, mreBH, mreC* and *mreD* deletion strains. The MreD-truncation mutant exhibits MreB delocalization under low Mg^{2+} concentration conditions. The effect was most apparent when cells were transferred from high Mg^{2+} medium (PAB + 20 mM $MgCl_2$) to low Mg^{2+} medium (PAB). Microscopy was carried out after 60 min incubation in low Mg^{2+} medium. To test the effect of valinomycin or nigericin, *B. subtilis* cells were grown in yeast extract-peptone medium supplemented with 50 mM Hepes-HCl pH 7.5, and 300 mM KCl.

ΔΨ of *B. subtilis* was dissipated by the addition of 30 μM valinomycin, and the ΔpH by addition of 5 μM nigericin directly to the culture medium[1], followed by 2 min incubation. Dissipation of the pmf in the different bacteria was established by the addition of 100 μM CCCP in all bacteria tested, as described before [1, 22, 23]. For inhibition of the dynamic movement of the cytoskeleton [24]., *B. subtilis* cells were incubated for 3 min with 2 μg/ml

vancomycin. For localization of Lipid II, cells were incubated for 5 min with 0.5 µg/ml fluorescein-labelled vancomycin (Van-FL) mixed with an equal concentration of unlabelled vancomycin [8].

Construction of strains

The strain encoding a truncation of *mreD* was constructed by amplification of an internal *mreD*-fragment using the oligonucleotides mreD-for, and mreD-rev1-157 (see Table S3), followed by cloning into pMutin4 [25] using restriction sites *Hin*dIII and *Bam*HI. Finally, the plasmid was integrated into *B. subtilis* 168 resulting in strain HS32 that encodes a C-terminal 15 amino acid truncation of MreD. Strain HS31 was constructed as a control to rule out possible polar effects of the pMutin4 integration. In this case, the intact (non-truncated) 3'-end of *mreD* was amplified using oligonucleotides mreD-for and mreD-rev1-172, followed by cloning and integration into *B. subtilis* 168. As a result, this strain does not carry a truncation of MreD but contains an integrated pMutin4 plasmid in the same locus.

The strain *B. subtilis* HS37 encoding GFP-MreB with a GFP_{A206K} exchange to prevent dimerization of GFP, was constructed by quick change method using primers GFPA206K-for and GFPA206K-rev followed and integration into the *amyE* locus of *B. subtilis* 168.

In order to analyse the CCCP-dependent localization of membrane proteins in the absence of MreB-homologs, an exchange of resistance markers was necessary. For this, the *amyE*-integration plasmid pSG1154 [26] was PCR-linearized using oligos pSG1154-for/pSG1154-rev, and tetR amplified from pBEST309 [27] using oligos tetR-for/tetR-rev. The PCR products were fused using In-Fusion HD Plus restriction free cloning kit (Clontech) resulting in pSG1154tetR. The protein-GFP fusions were amplified from chromosomal DNA of the corresponding *B. subtilis* strains using oligos Pxyl-for/GFP-rev, and integrated into pSG1154tetR PCR-linearized with oligos pSG1154-for2/pSG1154-rev2 using In-Fusion

cloning. The resulting plasmids were sequenced, and integrated into *B. subtilis* genome resulting in strains HS38-HS42. At last, the *mreB*-homologs were successively deleted in the order Δ*rsgI::spc*, Δ*mreBH::erm*, Δ*mbl::cat* and Ω*neo3427* Δ*mreB* resulting in strains HS43-47.

SUPPLEMENTARY REFERENCES

1. Strahl H, Hamoen LW. Membrane potential is important for bacterial cell division. *Proc Natl Acad Sci U S A* **107**, 12281-12286 (2010).
2. Wasungu L, Stuart MCA, Scarzello M, Engberts JBFN, Hoekstra D. Lipoplexes formed from sugar-based gemini surfactants undergo a lamellar-to-micellar phase transition at acidic pH. Evidence for a non-inverted membrane-destabilizing hexagonal phase of lipoplexes. *Biochim Biophys Acta* **1758**, 1677-1684 (2006).
3. Silva JPN, Oliveira MECDR, Coutinho PJG. Characterization of mixed DODAB/monoolein aggregates using Nile Red as a solvatochromic and anisotropy fluorescent probe. *J Photoch Photobio A* **203**, 32-39 (2009).
4. G Greenspan P, Fowler SD. Spectrofluorometric studies of the lipid probe, nile red. *J Lipid Res* **26**, 781-789 (1985).
5. Barak I, Muchova K, Wilkinson AJ, O'Toole PJ, Pavlendova N. Lipid spirals in *Bacillus subtilis* and their role in cell division. *Mol Microbiol* **68**, 1315-1327 (2008).
6. Muchova K, Wilkinson AJ, Barak I. Changes of lipid domains in *Bacillus subtilis* cells with disrupted cell wall peptidoglycan. *Fems Microbiol Lett* **325**, 92-98 (2011).
7. Li Q, Lau A, Morris TJ, Guo L, Fordyce CB, Stanley EF. A syntaxin 1, G alpha(o), and N-type calcium channel complex at a presynaptic nerve terminal: Analysis by quantitative immunocolocalization. *J Neurosci* **24**, 4070-4081 (2004).
8. Daniel RA, Errington J. Control of cell morphogenesis in bacteria: Two distinct ways to make a rod-shaped cell. *Cell* **113**, 767-776 (2003).
9. Barbe V, *et al.* From a consortium sequence to a unified sequence: the *Bacillus subtilis* 168 reference genome a decade later. *Microbiology* **155**, 1758-1775 (2009).
10. Formstone A, Errington J. A magnesium-dependent *mreB* null mutant: implications for the role of *mreB* in *Bacillus subtilis*. *Mol Microbiol* **55**, 1646-1657 (2005).
11. Schirner K, Errington J. The cell wall regulator σI specifically suppresses the lethal phenotype of *mbl* mutants in *Bacillus subtilis*. *J Bacteriol* **191**, 1404-1413 (2009).
12. Kawai Y, Daniel RA, Errington J. Regulation of cell wall morphogenesis in *Bacillus subtilis* by recruitment of PBP1 to the MreB helix. *Mol Microbiol* **71**, 1131-1144 (2009).
13. Johnson AS, van Horck S, Lewis PJ. Dynamic localization of membrane proteins in *Bacillus subtilis*. *Microbiology* **150**, 2815-2824 (2004).
14. Meijer WJ, Serna-Rico A, Salas M. Characterization of the bacteriophage phi29-encoded protein p16.7: a membrane protein involved in phage DNA replication. *Mol Microbiol* **39**, 731-746 (2001).
15. Meile JC, Wu LJ, Ehrlich SD, Errington J, Noirot P. Systematic localisation of proteins fused to the green fluorescent protein in *Bacillus subtilis*: Identification of new proteins at the DNA replication factory. *Proteomics* **6**, 2135-2146 (2006).
16. Hunt A, Rawlins JP, Thomaides HB, Errington J. Functional analysis of 11 putative essential genes in *Bacillus subtilis*. *Microbiology* **152**, 2895-2907 (2006).
17. Salzberg LI, Helmann JD. Phenotypic and transcriptomic characterization of *Bacillus subtilis* mutants with grossly altered membrane composition. *J Bacteriol* **190**, 7797-7807 (2008).
18. Hachmann AB, Angert ER, Helmann JD. Genetic analysis of factors affecting susceptibility of *Bacillus subtilis* to daptomycin. *Antimicrob Agents Chemother* **53**, 1598-1609 (2009).
19. Kobayashi K, *et al.* Essential *Bacillus subtilis* genes. *Proc Natl Acad Sci U S A* **100**, 4678-4683 (2003).

20. Tauch A, Kirchner O, Loffler B, Gotker S, Puhler A, Kalinowski J. Efficient electrotransformation of *Corynebacterium diphtheriae* with a mini-replicon derived from the *Corynebacterium glutamicum* plasmid pGA1. *Curr Microbiol* **45**, 362-367 (2002).
21. Kreiswirth BN, *et al.* The toxic shock syndrome exotoxin structural gene is not detectably transmitted by a prophage. *Nature* **305**, 709-712 (1983).
22. Bayan N, Schrempp S, Joliff G, Leblon G, Shechter E. Role of the protonmotive force and of the state of the lipids in the *in vivo* protein secretion in *Corynebacterium glutamicum*, a gram-positive bacterium. *Biochim Biophys Acta* **1146**, 97-105 (1993).
23. Patton TG, Yang SJ, Bayles KW. The role of proton motive force in expression of the *Staphylococcus aureus cid* and *lrg* operons. *Mol Microbiol* **59**, 1395-1404 (2006).
24. Garner EC, Bernard R, Wang W, Zhuang X, Rudner DZ, Mitchison T. Coupled, circumferential motions of the cell wall synthesis machinery and MreB filaments in *B. subtilis*. *Science* **333**, 222-225 (2011).
25. Vagner V, Dervyn E, Ehrlich SD. A vector for systematic gene inactivation in *Bacillus subtilis. Microbiology* **144 (Pt 11)**, 3097-3104 (1998).
26. Lewis PJ, Marston AL. GFP vectors for controlled expression and dual labelling of protein fusions in *Bacillus subtilis*. *Gene* **227**, 101-110 (1999).
27. Itaya M. Construction of a novel tetracycline resistance gene cassette useful as a marker on the *Bacillus subtili*s chromosome. *Biosci Biotech Bioch* **56**, 685-686 (1992).